

Behaviour of Thin Aluminium Plates Subjected to Impact by Ogive-nosed Projectiles

M.A. Iqbal, N.K. Gupta and G.S. Sekhon

Indian Institute of Technology Delhi, New Delhi-110 016

ABSTRACT

A pneumatic gas gun has been used to fire ogive-nosed projectiles on aluminium plates (1mm) at varying impact velocities above the ballistic limit. Impact and residual velocities have been measured. Deformation of the target plate was studied. Experimental results formed the basis of a subsequent finite element analysis of the problem using the ABAQUS 6.3 code. The Johnson-Cook plastic flow and fracture model available in the code were utilised. Explicit finite element analysis has been performed to model the perforation phenomenon. Numerical results were significantly improved by reducing the element size up to a certain level beyond which no significant variation in the results was observed. Adaptive meshing has been found to be useful in obtaining the accurate results and avoiding the problem of premature termination of the program due to excessive element distortion. Experimental and numerical results are compared and a good agreement between the two has been found.

Keywords: Ogive-nosed projectiles, perforation, adaptive meshing, aspect ratio, Johnson-Cook model

1. INTRODUCTION

Structural impact is a highly complex problem. The projectile perforation of a plate is a very complicated issue due to the involvement of various mechanical phenomena. The subject has been studied by a number of investigators in the past few decades.

Calder and Goldsmith¹ studied the dynamic response of thin aluminum plates subjected to impact of cylindro-conical steel projectiles. They proposed a simplified model for central deflection of rigid-plastic linear work hardening material. Results obtained from the simplified model matched with the experimental results at higher velocities of impact.

Corran², *et al.* investigated the effect of projectile mass, nose shape, and hardness on the penetration

of steel and aluminium alloy plates of various thicknesses.

Levy and Goldsmith³ used blunt, spherical, and conical projectiles to measure impact load, permanent deflection, and strain in aluminium and mild steel plates. They observed that an increase in the projectile mass results in the decrease of the ballistic limit.

Landkof and Goldsmith⁴ studied petalling of thin metallic plates when struck by cylindro-conical projectiles. A model based on plastic hinge theory for a study of petal bending was made to obtain the absorbed energy during perforation. For verification of the residual velocity and other parameters predicted by the model, an experimental program was conducted. Good correlation was found between the experimental and the theoretical residual velocities except near the ballistic limit.

Gupta and Madhu^{5,6} carried out studies of the normal and oblique impact behaviour of ogive-nosed armour-piercing projectiles on a single and multi-layered metallic plates. Simple mathematical relations based on the experimental results were proposed for predicting the residual velocity, velocity drop, ballistic limit, and critical ricochet angle. It was found that the residual velocity for relatively thick plates in two layers was comparable to that in the case of a single plate of equal thickness. However for thin plates, the layered combination gave higher residual velocity. Again the residual velocity for spaced (layered) targets was higher than when the plates were in contact.

Piekutowski⁷, *et al.* conducted perforation tests on 6061-T651 aluminium plates by ogive-nosed steel rods in normal and oblique directions. Perforation equations were developed for predicting the ballistic limit and residual velocity.

Gupta⁸, *et al.* investigated the behaviour of single plates of aluminium of different thicknesses subjected to normal impact by ogive-nosed projectiles at velocities greater than their ballistic limit. They developed analytical expressions based on mechanics of deformation of the target plate and empirical relations for the determination of residual velocity and ballistic limit. These relations were found to fit the experimental results.

Chocron⁹, *et al.* conducted a numerical study on the impact of ogive-nosed projectiles against aluminium and steel targets. Simulation of the full projectile (jacket, lead nose, and core) showed that standard values for the erosion strain gave results that were incompatible with experiments for the plate-edge impact interaction.

Borvik^{10, 11}, *et al.* carried out experimental as well as numerical investigations on the impact of blunt, hemispherical and conical projectiles on steel plates. They found from experiments that at low velocities, the blunt projectiles were better penetrators than hemispherical and conical projectiles. However at higher impact velocities, conical projectiles require less energy to perforate the target. It was also found that finite element results were improved by reducing the element size. Adaptive meshing was

found to be useful in overcoming the numerical problems.

Different aspects of the problem of perforation of metallic plates by projectiles have been studied by several researchers. However, there are relatively few studies on the finite element simulation of the phenomenon in the published literature. In the past, more attention was given to experimentally investigate the impact behaviour of target and projectile and to construct approximate analytical models. The use of the numerical technique in perforation problems was initiated around 1990. However, reported studies in which experimental results are directly compared with those found from finite element simulation are rather few. This is perhaps due to the fact that a typical numerical simulation, requires a number of material parameters that need to be determined from material tests and the process to obtain these is quite complicated.

In the present study, a series of experiments involving impact of ogive-nosed bullets on 1100-H12 aluminium plates (1 mm) have been conducted. Impact and residual velocities have been measured. Deformation mechanism of the target has been analysed. A finite element analysis the perforation phenomenon has also been carried out using the ABAQUS 6.3 code². It was observed that as the velocity of impact was increased, velocity drop of the projectile decreased. Element size was found to affect the accuracy of the numerical results.

2. EXPERIMENTAL INVESTIGATION AND RESULTS

2.1 Experimental Investigation

Experimental investigations were carried out using a pneumatic gas gun (Fig. 1). An ogive-nosed steel projectile of diameter (15 mm) was fired on 1100-H12 aluminium plates (1 mm) at varying impact velocity. The plate was clamped to a rigid bracket by means of 16 steel bolts arranged on a pitch circle of diameter 230 mm. Mass of the projectile was 55 g. Geometry of the projectile is shown in Fig. 2. The projectile velocity was measured with the help of a simple photo gate type arrangement comprising three infrared light emitting diodes and

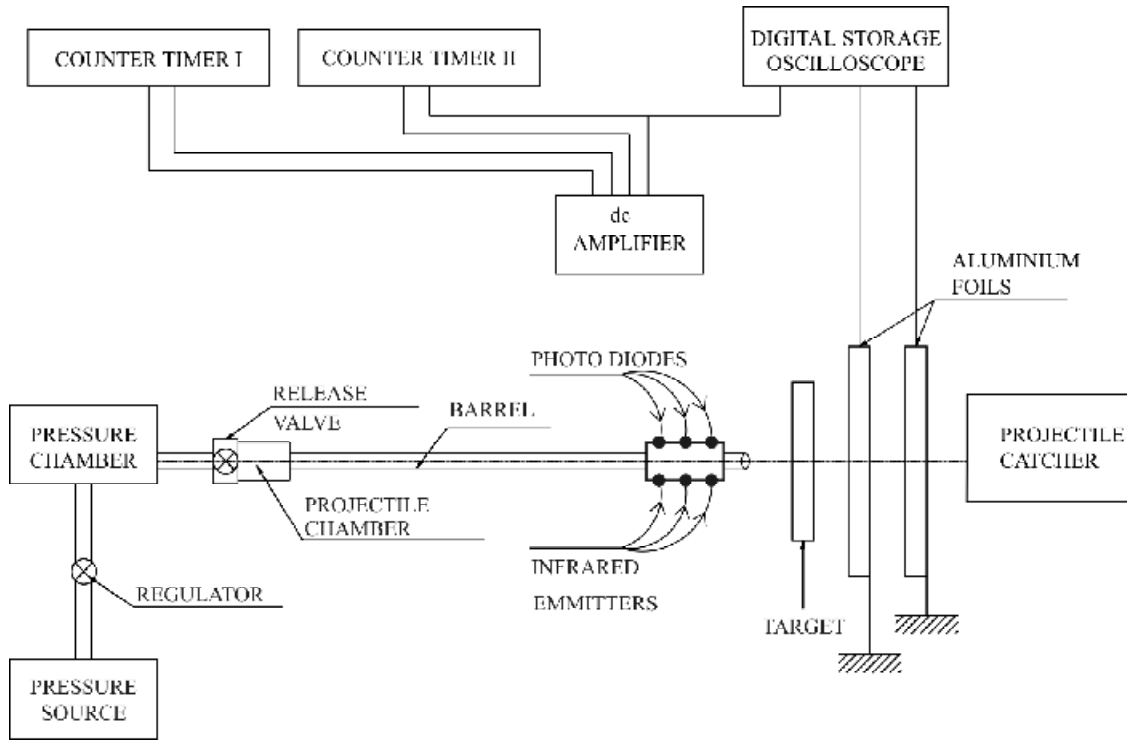


Figure 1. Schematic diagram of the experimental setup.

three photodiodes. Residual velocity of the projectile was measured with the help of two sets of aluminium foil screens of $6\ \mu\text{m}$ thickness, placed behind the target plate. The target plate was circular, of diameter (255 mm) cut from an aluminium sheet. To ensure that the projectile hits the target normally, the distance between the end of the gun muzzle and the target plate was kept small. The projectile was oil-quenched to a Rockwell hardness, R_c of 52 before it was used. In all the experiments, projectile velocity was kept above the ballistic limit. All the parameters, except for firing velocity, were kept constant. Experimental results are shown in Table 1.

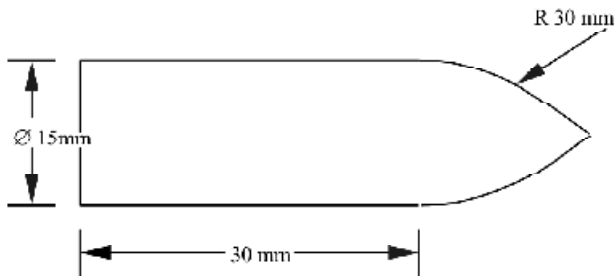


Figure 2. Geometry of ogive-nosed projectile.

2.2 Results

It was observed that the velocity drop of the projectile decreased slightly with an increase in the impact velocity. The global bending of the target measured using a mechanical dial gauge system decreased with increase in the impact velocity. As a result, the velocity drop of the projectile also decreased. The target failure was due to ductile hole enlargement, and plug formation was absent. This failure mode is typical of impact by ogival- or conical-nosed projectile. The nose of the projectile

Table 1. Observed values of impact velocity V_i , residual velocity V_r , velocity drop V_d , energy absorbed by the target E_{abs} , and maximum deflection of the target plate w_{max}

Test No.	V_i (m/s)	V_r (m/s)	V_d (m/s)	E_{abs} (J)	w_{max} (mm)
1	103.72	92.11	11.61	62.54	5.75
2	97.23	85.66	11.96	58.19	6.15
3	82.97	71.21	12.35	49.86	6.91
4	81.91	70.45	12.71	48.01	7.18
5	73.31	59.38	13.92	50.80	7.88
6	65.80	52.66	16.11	42.78	8.04

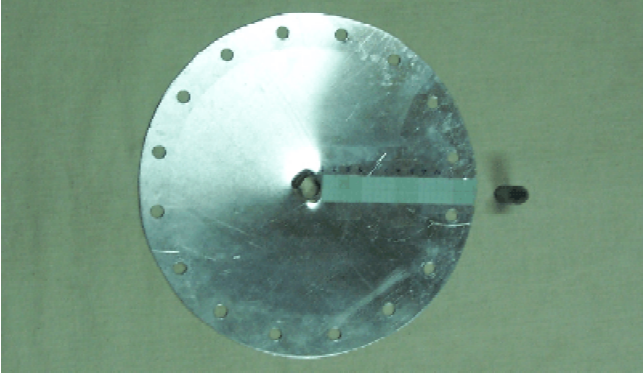


Figure 3. Photograph of the projectile and the deformed specimen.

first formed a minute hole in the target along the axis of the projectile trajectory. The same got enlarged due to the high radial pressure as the projectile passed through it. The target also deformed first at its centre in the shape of a crater around the projectile nose. As the projectile moved forward, the tip of the projectile busted through the plate and emerged from the rear side of the target. The crack which was initiated at the tip of the crater propagated and formed petals. These petals were bent during the onward movement of the projectile by as much as 90° from the surface of plate. In the present study, four petals were formed. Thinning of the target plate was observed in the petalling region from the root of the petal to its tip. Maximum thinning occurred at the tip of the petals. A typical deformed target plate and the projectile used in the present study are shown in Fig. 3.

3. MATERIAL MODELLING

The most important factor affecting the results of a numerical study is the selection of a proper material model. A number of models have been described in the literature some of which are quite complex¹³. Due to difficulties involved in obtaining the material constants, simpler models are, however, preferred. The ABAQUS 6.3 code¹² used in the present study for finite element simulation of the perforation phenomenon has an in-built option of the material model proposed by Johnson and Cook¹⁴. It allows for linear thermoelasticity, yielding, the associated flow rule, isotropic strain hardening, strain rate hardening, softening due to adiabatic

heating, softening due to isotropic damage evolution, and a failure criterion. According to the Johnson and Cook model¹², the equivalent stress $\bar{\sigma}$ may be expressed as follows:

$$\bar{\sigma} = \left[A + B(\bar{\epsilon}^{pl})^n \right] \left[1 + C \ln \left(\frac{\dot{\bar{\epsilon}}^{pl}}{\dot{\epsilon}_0} \right) \right] (1 - \hat{\theta}^m) \quad (1)$$

where A, B, C, n , and m are the material parameters, $\bar{\epsilon}^{pl}$ is the equivalent plastic strain, $\dot{\bar{\epsilon}}^{pl}$ is the equivalent plastic strain rate, $\dot{\epsilon}_0$ is the reference strain rate, and $\hat{\theta}$ is the nondimensional temperature defined as

$$\hat{\theta} = (\theta - \theta_{transition}) / (\theta_{melt} - \theta_{transition})$$

$$\theta_{transition} \leq \theta \leq \theta_{melt} \quad (2)$$

where θ is the actual temperature, θ_{melt} is the melting point temperature, and $\theta_{transition}$ is the transition temperature at or below which there is no temperature dependence.

The fracture model proposed by Johnson and Cook¹⁵ considered the effect of stress triaxiality, strain rate, and temperature on the equivalent failure strain. The failure criterion is based on the value of the equivalent plastic strain at element integration points. Failure is assumed to occur when the so-called damage parameter, ω , exceeds unity¹². The damage parameter, ω , is defined as

$$\omega = \sum \left(\frac{\Delta \bar{\epsilon}^{pl}}{\bar{\epsilon}_f^{pl}} \right) \quad (3)$$

where $\Delta \bar{\epsilon}^{pl}$ is an increment of the equivalent plastic strain, $\bar{\epsilon}_f^{pl}$ is the strain at failure, and the summation is performed over all the increments in the analysis.

The strain at failure, $\bar{\epsilon}_f^{pl}$, is assumed to be dependent on a nondimensional plastic strain rate, $\dot{\bar{\epsilon}}^{pl} / \dot{\epsilon}_0$, a dimensionless pressure-deviatoric stress ratio, p/q (where p is the pressure stress and q is the

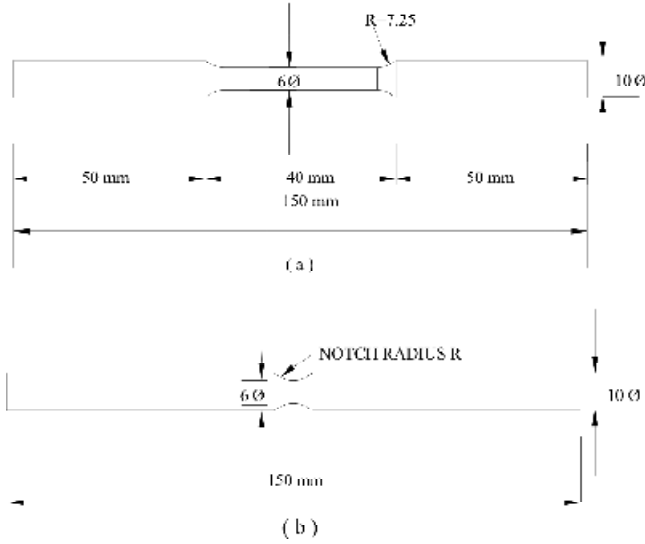


Figure 4. Geometry of the tensile test specimens: (a) smooth specimen and (b) notched specimen.

Von-Mises stress), and the nondimensional temperature, $\hat{\theta}$, defined earlier. The different dependencies are assumed separable and are of the form¹²:

$$\bar{\epsilon}_f^{pl} = \left[d_1 + d_2 \exp\left(d_3 \frac{p}{q}\right) \right] \left[1 + d_4 \ln\left(\frac{\dot{\epsilon}^{pl}}{\dot{\epsilon}_0}\right) \right] (1 + d_5 \hat{\theta}) \quad (4)$$

where d_1 through d_5 are the material constants. Whenever the failure criterion is met at any point, the deviatoric components of stress at that point are set to zero and remain zero during the remainder of the analysis. The element kill algorithm available in the software¹² has been used to delete the failed elements from the mesh. It ensures that the pressure stress in killed elements is made to vanish during the subsequent analysis.

The different parameters for the test material were found from mechanical tests. Round tensile specimens of the test material (aluminium 1100-H12) were prepared [Fig. 4(a)]. Uniaxial tensile tests were carried out on a Zwick Z250/SN5A universal testing machine at a fixed strain rate of $4.16 \times 10^{-4} \text{ s}^{-1}$. Values of the modulus of elasticity, Poisson's ratio and yield stress were determined. Diameter reduction was observed till the fracture

occurred, and true strain was obtained from the following expression:

$$\bar{\epsilon}_f^{pl} = 2 \ln(D_0/D) \quad (5)$$

where D_0 is the initial diameter and D is the current diameter of the specimen. True stress was found as F/A , where F is the measured force in Newton and A is the actual area in (millimeter)² of the specimen. The stress in the tensile specimen is practically uniaxial before the onset of necking. However after the necking starts, the stress state becomes three-dimensional. Therefore, Bridgman correction¹⁶ was applied to the measured true stress. The corrected equivalent stress (σ_{eq}) was calculated using the following expression:

$$\frac{\bar{\sigma}_x}{\sigma_{eq}} = \left(1 + \frac{2R}{a}\right) \ln\left(1 + \frac{a}{2R}\right) \quad (6)$$

where $\bar{\sigma}_x$ is the measured true stress, R is the radius of curvature of the neck and a is the current radius of specimen in the necked region. During the experiments, reduction of the specimen diameter was measured but the radius of curvature was not obtained. Instead, the ratio of a/R was obtained using the empirical expression given by Le Roy¹⁷, *et al.* as

$$\frac{a}{R} = \begin{cases} 0 & \text{for } \epsilon \leq \epsilon_u \\ 1.11(\epsilon - \epsilon_u) & \text{for } \epsilon > \epsilon_u \end{cases} \quad (7)$$

where ϵ_u and ϵ are the ultimate and the actual true strains of the specimen, respectively. The factor 1.11 in the above expression, although validated for steel, was considered suitable for aluminium also. The corrected true stress-true strain curve is shown in Fig. 5. The above stress-strain curve was next used to compute the values of the strain-hardening constants B and n using the least squares method. The Johnson-Cook constants, C and m in the next two brackets of equivalent stress expression Eqn (1) were taken from the work of Clausen¹³, *et al.* Although the aluminium alloy used in their experimentation was comparatively rich in magnesium but these values are assumed to be approximately

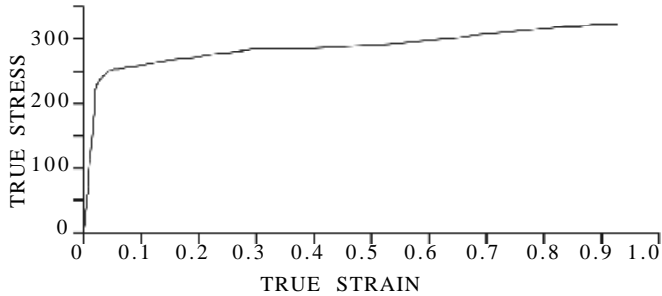


Figure 5. True stress-true strain curve of the target material.

valid for the present material also. Tests were also performed on artificial notched specimens [Fig. 4(b)] with three different notch radii, namely 2.0 mm, 0.8 mm, 0.4 mm. An artificial notch produced an initial triaxiality different from that of a smooth specimen where triaxiality was initiated only after the commencement of necking. Bridgman's relationship given below was used to correlate the initial notch radius R and the maximum stress triaxiality ratio σ_{max}^* as

$$\sigma_{max}^* = \frac{1}{3} + \ln \left(1 + \frac{a}{2R} \right) \quad (8)$$

The triaxiality ratios obtained from the above expression along with the fracture strains values of different specimens were used to obtain the parameters d_1 , d_2 , d_3 and Eqn (4) using least squares method. The value of d_4 , which expresses the strain rate effect on the equivalent fracture strain was taken from the work of Clausen¹³, *et al.* The parameter d_5 was not evaluated since adiabatic temperature rise was not significant in the context of the projectile impact on thin plates. The material parameters found during the present study are shown in Table 2.

4. NUMERICAL INVESTIGATIONS AND RESULTS

4.1 Numerical Investigation

Numerical investigation was carried out using the finite element code¹² ABAQUS 6.3. Explicit time integration was performed, using the central differences scheme for each increment.

An axisymmetric model of the bullet and the plate was created using the preprocessing module of the software (Fig. 6). The target was modelled

Table 2. Material parameters for the tests specimens

Parameter	Symbol	Value
Modulus of elasticity	E (N/mm ²)	65.762 x10 ³
Poisson's ratio	ν	0.300
Density	ρ (kg/m ³)	2700.000
Yield stress	A (N/mm ²)	148.361
	B (N/mm ²)	345.513
	n	0.183
	C	0.001
Reference strain rate	$\dot{\epsilon}_0$	1.000 s ⁻¹
	m	0.859
	θ_{melt} (K)	893.000
	$\theta_{transition}$ (K)	293.000
	d_1	0.071
	d_2	1.248
	d_3	-1.142
	d_4	0.147
	d_5	0.0

as a deformable body and the material properties were assigned to it. The bullet was modelled as a rigid body having a single-node reference point with assigned mass and initial velocity. Four-noded axisymmetric elements and single-point integration were used for the analysis. Mesh was refined in the influence region. Aspect ratio of the elements was maintained close to unity in the influence region though it was allowed to increase towards the periphery of the plate. A total number of elements in the problem domain was 8360. There were 20 elements in the thickness direction of the plate. The target plate was fixed at the support placed at the radius of 115 mm. Contact between the bullet and the plate was modelled using a kinematic contact algorithm, considering the bullet as the master surface and the influence zone of the target plate as the slave surface. Frictional effects were considered negligible. Adaptive meshing was employed to avoid problems associated with excessive distortion of elements in the mesh. (The adaptive meshing available in the ABAQUS does not change the number of elements or their nodal connectivity). The so-called lagrangian adaptive meshing was used in the region of the target plate directly in

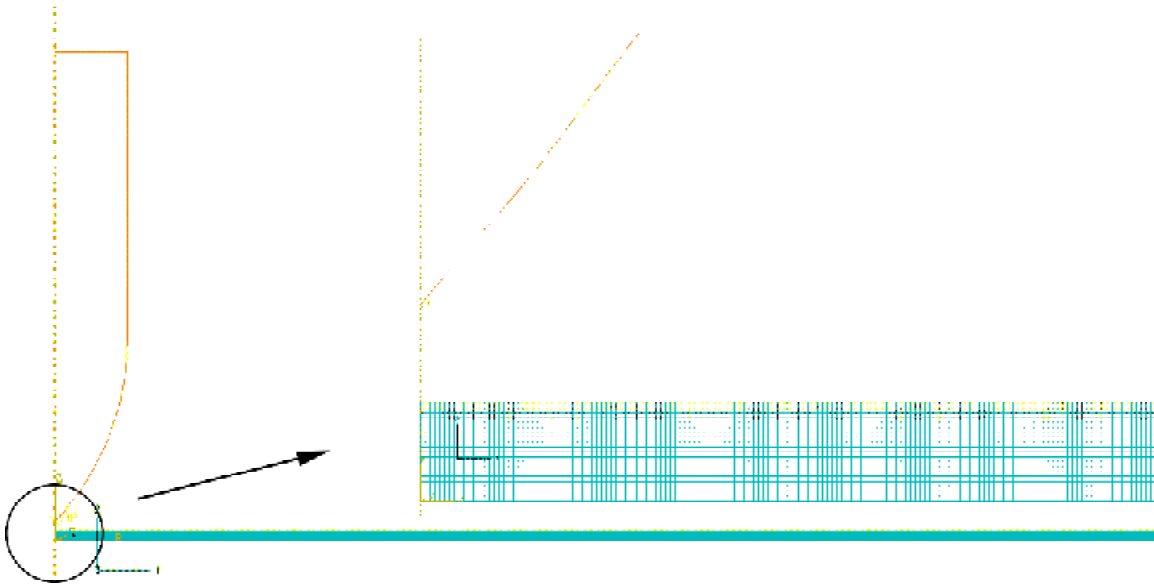


Figure 6. Proposed finite element model.

front of the projectile and equal to its radius. Ten mesh sweeps were performed at each increment. Solution convergence was verified by carrying out computations using higher mesh density. The refined mesh comprised a total of 10752 elements with 24 elements in the thickness direction. The values of the residual velocity obtained (Table 3) using the refined mesh agreed closely with the corresponding values found by the mesh described earlier.

4.2 Results

Simulations were carried out at different velocities of impact. Table 4 lists the predictions of the residual projectile velocity, perforation time and target deformation as a result of impact. Global deformation of the plate was found to decrease with an increase of the impact velocity in the same fashion as observed from the experiments. But the computational results predicted higher values of global deformation than

the actual. Experimentally and numerically obtained residual velocities have been compared in Fig.7. The residual velocities predicted by the numerical model are lower than the actual. As the impact velocity was increased, the difference between the actual and the predicted velocity drop curves, shown in Fig. 8, got reduced till finally both the

Table 3. Mesh-independent numerical results (using a refined mesh)

V_i (m/s)	V_r (m/s)	V_{drop} (m/s)	E_{abs} (J)	P_f (s)	CPU (h)	w_{max} (mm)
103.72	90.87	12.43	66.41	7.0e-4	22.83	6.09

curves became almost parallel. At the lowest impact velocity (65.8 m/s), the difference was nearly 17.4 per cent, however, this got reduced to almost 1.4 per cent as the impact velocity increased beyond 100 m/s, presumably due to some unaccounted

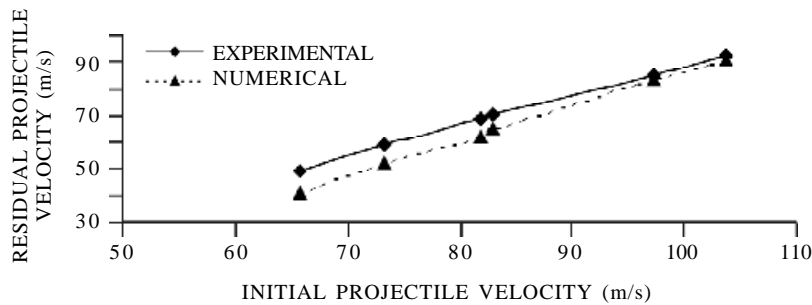


Figure 7. Variation of residual velocity with impact velocity.

Table 4. Predicted values of impact velocity V_i , residual velocity V_r , velocity drop V_d , energy absorbed by the target E_{abs} , full perforation time of the target P_f , CPU time for the analysis and maximum deflection of the target plate w_{max}

Test No.	V_i (m/s)	V_r (m/s)	V_d (m/s)	E_{abs} (J)	P_f (s)	CPU (h)	w_{max} (mm)
1	103.72	90.85	12.85	68.78	7.0e-4	15.20	5.81
2	97.23	83.25	13.97	69.38	7.5e-4	15.31	6.08
3	82.97	65.71	17.26	70.57	9.0e-4	20.16	8.53
4	81.91	62.27	19.63	77.86	9.0e-4	20.22	8.55
5	73.31	52.67	20.62	71.46	9.5e-4	23.33	9.13
6	65.8	41.04	24.76	72.75	11.0e-4	26.81	9.72

dependence of material parameters on the rate of loading.

Figure 9 shows the Von-Mises stress (effective stress) contours in the target plate due to projectile impact. When the projectile comes in contact with the target, it kills few elements adjacent to its tip. Further movement of the projectile bends the target. The bending was, however, more pronounced in the contact zone than elsewhere. Maximum Von-Mises stress developed in the region of the target that was in contact with the projectile. The effective stress increased with an increase of perforation of the plate by the projectile. The portion of the target that was in contact with the projectile bent in the shape of the projectile, and cracked apart to form petals. The peak value of the effective stress was reached when the whole of the ogival portion of the projectile perforated the target. At this instant, the target region that was in contact with the projectile body was bent approximately at 90° from the surface

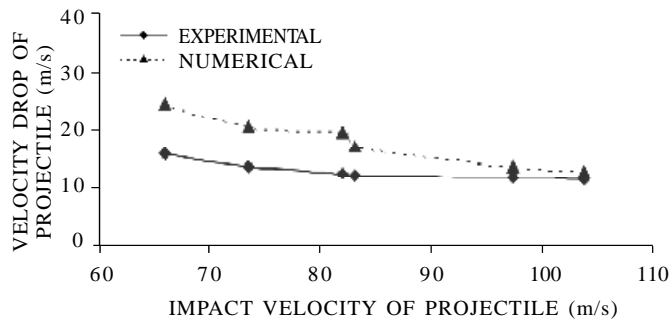


Figure 8. Variation of velocity drop with impact velocity.

of plate. The predicted failure pattern of the target was exactly the same as the actual failure pattern.

Shear stress contours have been plotted in Fig. 10. When the projectile hit the target, maximum shear stress developed on the front side of the target in the bent region at a point located slightly outside of the contact region with the projectile. The value of the maximum shear stress increased with the onward movement of the projectile and reached a peak value at the instant when the full ogival portion of the projectile had perforated the target. Afterwards, the maximum shear stress value tended to decrease with further movement of the projectile.

5. CONCLUSION

Experiments were carried out on aluminium plates of thickness 1 mm using ogive-nosed projectile. Residual velocities of the projectile were measured. At low velocities of impact, the velocity drop is greater and vice-versa. The target fails through ductile hole enlargement. It was observed that greater energy is absorbed in localised deformation than in global bending. Global dishing of the target plate is found to decrease with an increase in the impact velocity. Four petals are formed at all the impact velocities. Thinning of the target plate occurs in the petalling region. Thinning start at the root of the petal and is the maximum at its tip.

Finite element simulations have been performed using the explicit solution technique of the ABAQUS finite element code. Material modelling has been performed using a coupled model of plastic flow and fracture, originally proposed by Johnson-Cook. The numerical simulation describes the observed perforation phenomenon well. However, predicted global dishing of the target is found to be somewhat higher than the actual global dishing.

The size of the element is found to be a significant factor affecting the reliability of the computational results. Adaptive meshing has been found as a useful tool for avoiding excessive element distortion and reducing the computational cost. Experimental and computational results presented in Tables 1 and 4, respectively are seen to match well.

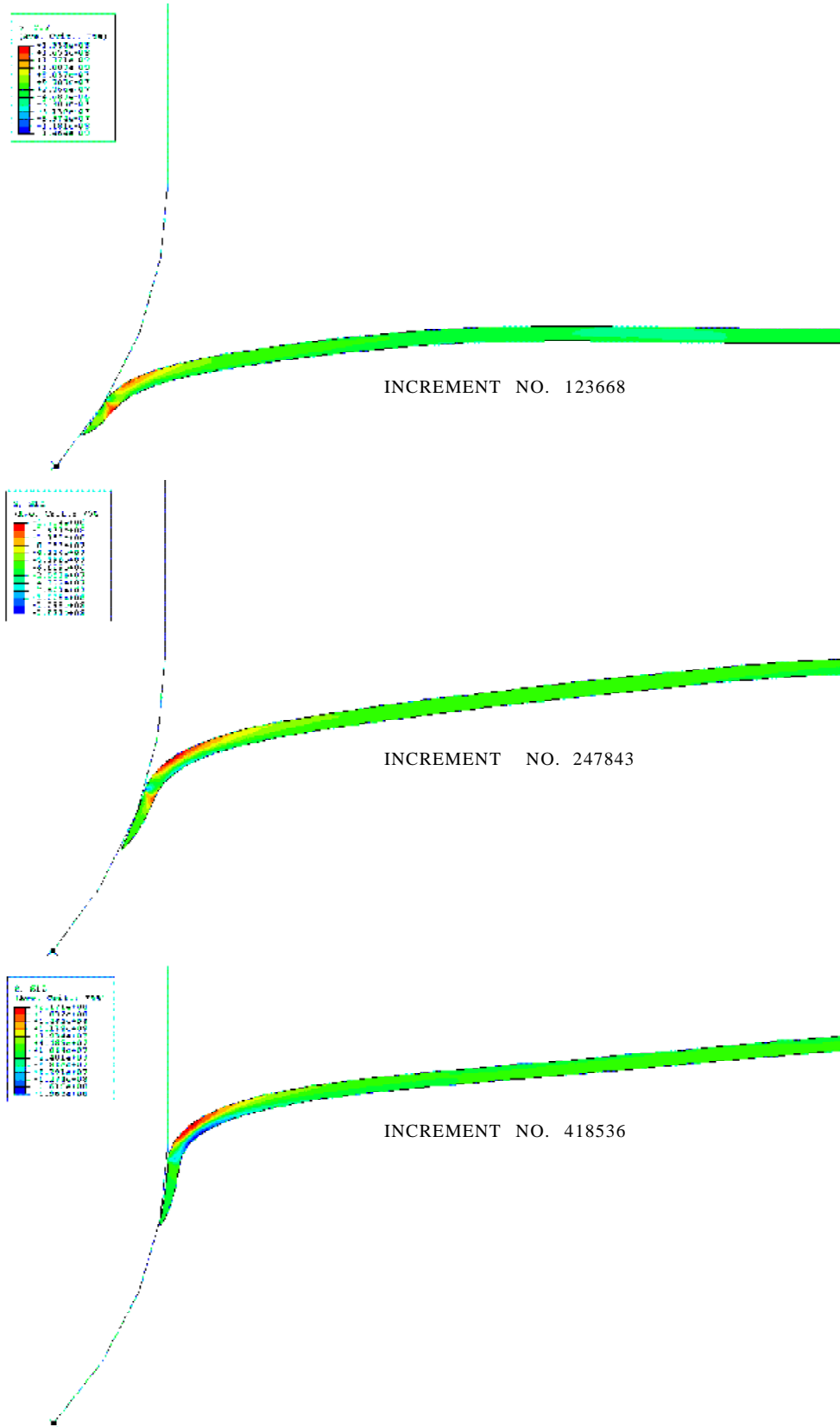


Figure 10. Predicted shear stress contours.

REFERENCES

1. Calder, C.A. & Goldsmith, W. Plastic deformation and perforation of thin plates resulting from projectile impact. *Int. J. Solids Struct.*, 1971, **7**, 863–81.
2. Corran, R.S.J.; Shadbolt, P.J. & Ruiz, C. Impact loading on plates—an experimental investigation. *Int. J. Impact Engg.*, 1983, **1**, 3–22.
3. Levy, N. & Goldsmith, W. Normal impact and perforation of thin plates by hemispherically-tipped projectiles—II, experimental results. *Int. J. Impact Engg.* 1984, (2), 299–324.
4. Landkof, B. & Goldsmith, W. Petalling of thin, metallic plates during penetration by cylindro-conical projectiles. *Int. J. Solids Struct.*, 1985, **21**, 245–66.
5. Gupta, N. K. & Madhu, V. Normal and oblique impact of a kinetic energy projectile on mild steel plates. *Int. J. Impact Engg.*, 1992, **12**, 333–43.
6. Gupta, N.K. & Madhu, V. An experimental study of normal and oblique impact of hard-core projectile on single and layered plates. *Int. J. Impact Engg.*, 1997, **19**, 395–14.
7. Piekutowski, A. J.; Forrestal, M. J.; Poormon, K. L. & Warren, T. L. Perforation of aluminium plates with ogive-nose steel rods at normal and oblique impacts. *Int. J. Impact Engg.*, 1996, **18**, 877-87.
8. Gupta, N. K.; Ansari, R. & Gupta, S. K. Normal impact of ogive-nosed projectiles on thin plates. *Int. J. Impact Engg.*, 2001, **25**, 641–60.
9. Chocron, S.; Anderson (Jr), E. C.; Grosch, D. J. & Propelar, C. H. Impact of 7.62 mm AMP2 projectile against the edge of a metallic target. *Int. J. Impact Engg.*, 2001, **25**, 423–37.
10. Borvik, T.; Langseth, M.; Hopperstad, O.S.; & Malo, K.A. Perforation of 12 mm thick steel plates by 20 mm diameter projectiles with flat, hemispherical and conical noses: Part I: Experimental study. *Int. J. Impact Engg.*, 2002, **27**, 19–35.
11. Borvik, T.; Hopperstad, O.S.; Berstad, T. & Langseth, M. Perforation of 12 mm thick steel plates by 20 mm diameter projectiles with flat, hemispherical and conical noses: Part II: Numerical simulations. *Int. J. Impact Engg.*, 2002, **27**, 37–64.
12. ABAQUS/Explicit User's Manual, Vol. I-II; Version 6.3, 2002.
13. Clausen, A.H.; Borvik, T.; Hopperstad, O.S. & Benallal, A. Flow and fracture characteristics of aluminium alloy AA5083–H116 as function of strain rate, temperature and triaxiality. *Mat. Sci. Engg.*, 2004, (A364), 260-72.
14. Johnson, G.R. & Cook, W.H. A constitutive model and data for metals subjected to large strains, high strain rates, and high temperatures. *In Proceedings of the Seventh International Symposium on Ballistics*, The Hague, 1983.
15. Johnson, G.R. & Cook, W.H. Fracture characteristics of three metals subjected to various strains, strain rates, temperatures, and pressures. *Engg. Fract. Mech.*, 1985, **21** (1), 31-48.
16. Bridgman, P.W. *Studies in large plastic flow and fracture*. McGraw-Hill, New York, 1952.
17. Le Roy, G.; Embury, J.D.; Edwards, G. & Ashby, M.F. *Acta Metallurgica*, 1981, **29**, 1509.
18. Zukas, J.A.; Nicholas, T.; Swift, H.F.; Greszczuk, L.B. & Curran, D.R. *Impact Dynamics*, New York, Wiley, 1982.

Contributor



Prof N.K. Gupta is internationally well-recognised for his researches in the area of large deformations of metals and composites at low, medium, and high rates of loading. His researches find applications in design for crashworthiness of aircraft and road vehicles, design of protective armour, and the analysis of metal forming problems. He has published extensively in renowned international journals, guided researchers at PhD and MTech levels, and undertaken national and international research and consultancy projects. He has been Visiting Professor/Fellow/invited to deliver inaugural, keynote and guest lectures in universities in all the five continents. Currently, he is Henry Ford chair Emeritus Professor at the Indian Institute of Technology Delhi.